Supporting information for

Lithium transport in $Li_{4.4}M_{0.4}M'_{0.6}S_4$ (M= Al^{3+}, Ga^{3+} and M'= Ge^{4+}, Sn^{4+}): Combined crystallographic, conductivity, solid state NMR and computational studies

Bernhard T. Leube[1], Kenneth K. Inglis[1], Elliot Carrington[1], Paul M. Sharp[1], J. Felix Shin[1], Alex R. Neale[1,2], Troy D. Manning[1], Michael J. Pitcher[1], Laurence J. Hardwick [1,2], Matthew S. Dyer[1], Frédéric Blanc[1,2], John B. Claridge[1] and Matthew J. Rosseinsky[1]

[1]*Department of Chemistry, University of Liverpool, Crown Street, L69 7ZD, UK*

[2]*Stephenson Institute for Renewable Energy, University of Liverpool, Peach Street, L69 7ZF, UK*

Contents:

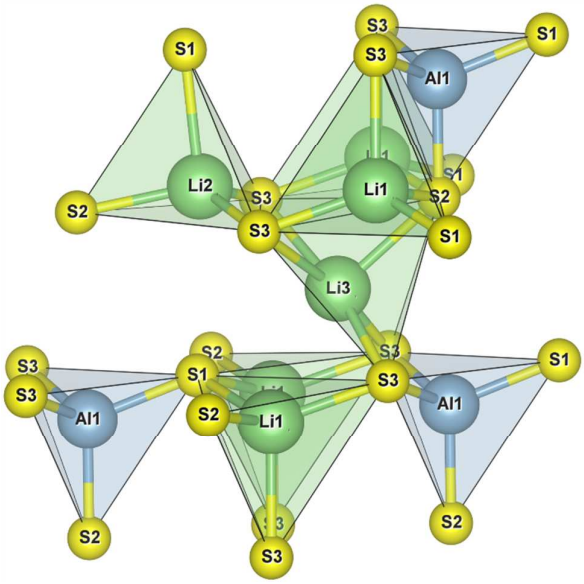

Figure S1: Fragment of the Li_5AlS_4 structure showing the displacement of Li3 towards S2, away from the triangular face shared by two Li1 tetrahedra and one Al1 tetrahedron towards a face containing two Li1 and a Li2 tetrahedra. The displacement is also towards S2 in order to maximise the bonding as this sulfur is displaced out of the hcp layer towards Al1 due to the bonding requirements of Al1.

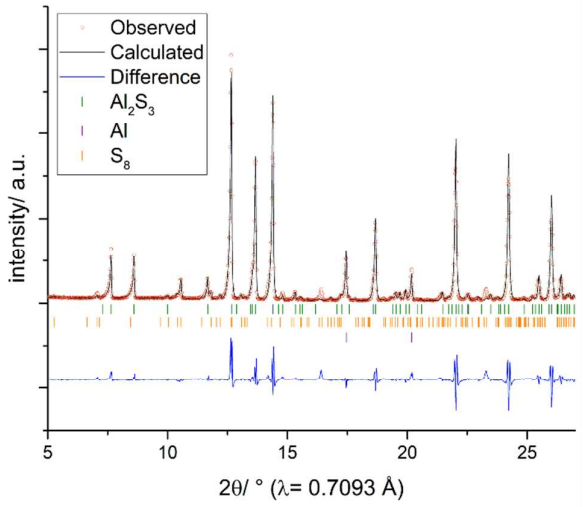

Figure 2: Rietveld fit to the laboratory PXRD pattern of Al_2S_3 used in the synthesis. Besides Al_2S_3 (85.0 wt%), Al(7.5 wt%) and S_8 (7.5 wt%) can be identified. The positons of calculated Bragg reflections are shown by tick marks (green: Al_2S_3, purple: Al, orange: S_8).

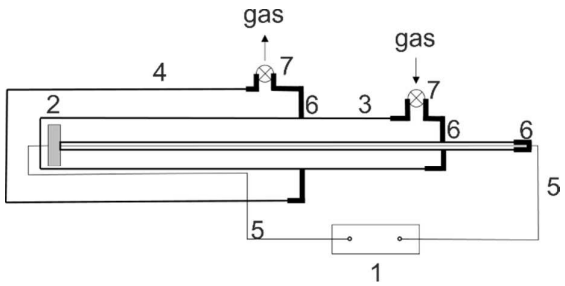

1: impedance spectroscopy instrument
2: sample
3: inner tube
4: outer tube
5: Pt wire
6: Ultra-Torr® vacuum fitting
7: valve

Figure S3: Schematic diagram of the custom built AC-impedance sample holder, which was used to measure samples under a stream of argon.

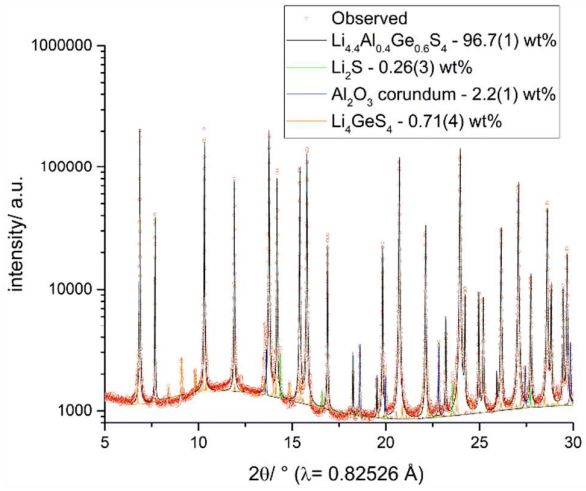

Figure S4: Multi-phase Rietveld fit to the SXRD pattern of $Li_{4.4}Al_{0.4}Ge_{0.6}S_4$ sample used for elemental analysis and NMR experiments (synthesised using commercial Li_2S and Ge without further purification); the intensities are plotted in a logarithmic scale. The colour code for the Rietveld fits of the individual components is: black: $Li_{4.4}Al_{0.4}Ge_{0.6}S_4$, green: Li_2S, blue: Al_2O_3, orange: Li_4GeS_4.

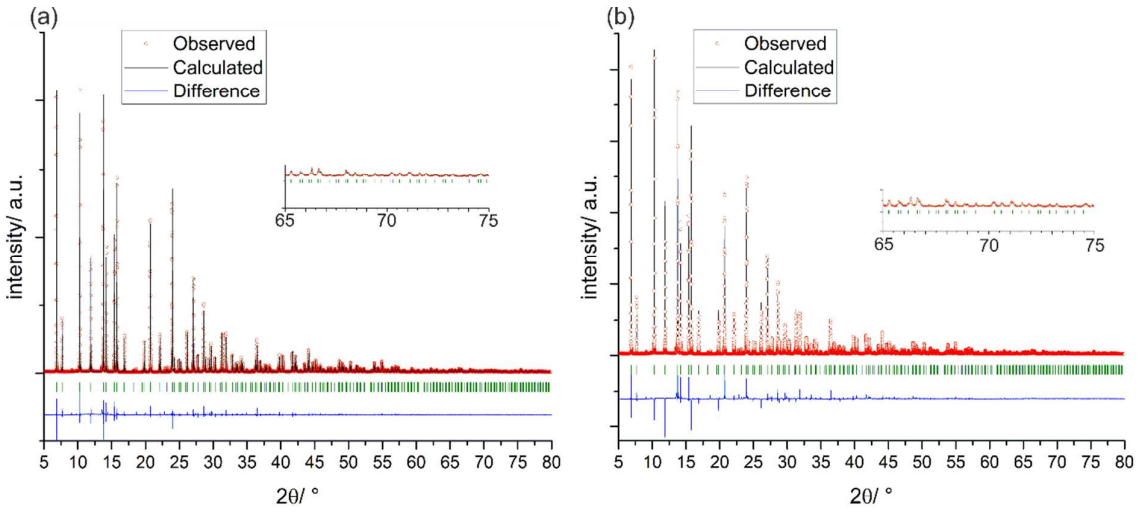

Figure S5: Fits of the lithium-free preliminary model of $Li_{4.4}Al_{0.4}Ge_{0.6}S_4$, taking into account only the sulphur-heavy metal framework without any lithium sites, against SXRD data (I11 beamline, MAC detector, λ= 0.82526 Å, room temperature). The positons of calculated Bragg reflections are shown by tick marks, the insets show the good fit to high angle data. (a) Pawley fit, R_{wp}= 11.72, χ^2= 40.424 (b) Rietveld fit, R_{wp}= 13.54, χ^2= 51.471.

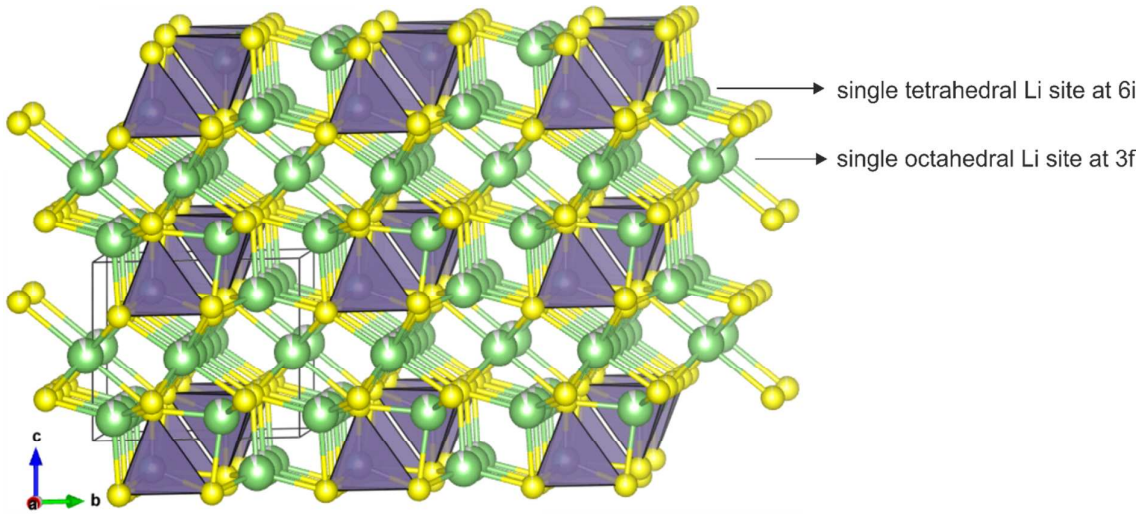

Figure S6: Structural model of $Li_{4.4}Al_{0.4}Ge_{0.6}S_{0.4}$ from SXRD with preliminary/approximate lithium sites (corresponding to the Rietveld fit in Figure S5). Atoms and polyhedra are coloured as follows: yellow = sulphur, green = lithium, purple = mixed Al^{3+}/Ge^{4+} site. Partially occupied atoms are coloured to represent fractional occupancies.

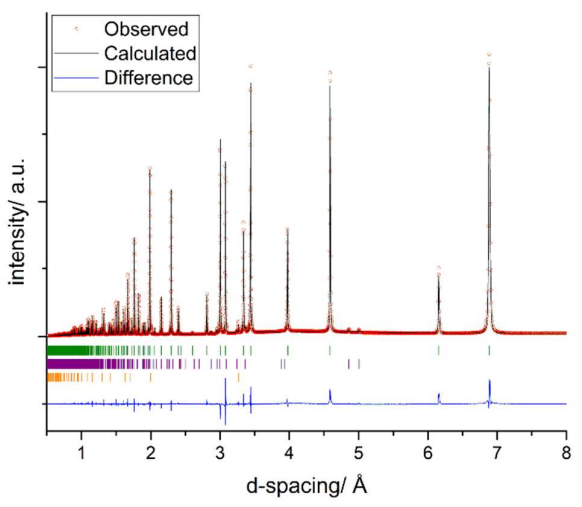

Figure S7: Ambient temperature Rietveld refinements of $^{7}Li_{4.4}Al_{0.4}Ge_{0.6}S_4$ (synthesised using purified reactants) against SXRD data (I11 beamline, MAC-detector, λ= 0.824878 Å), using the final NPD-derived model with three Li sites. The positons of calculated Bragg reflections are shown by tick marks (green: $^{7}Li_{4.4}Al_{0.4}Ge_{0.6}S_4$, purple: $LiAlS_2$, orange: Ge).

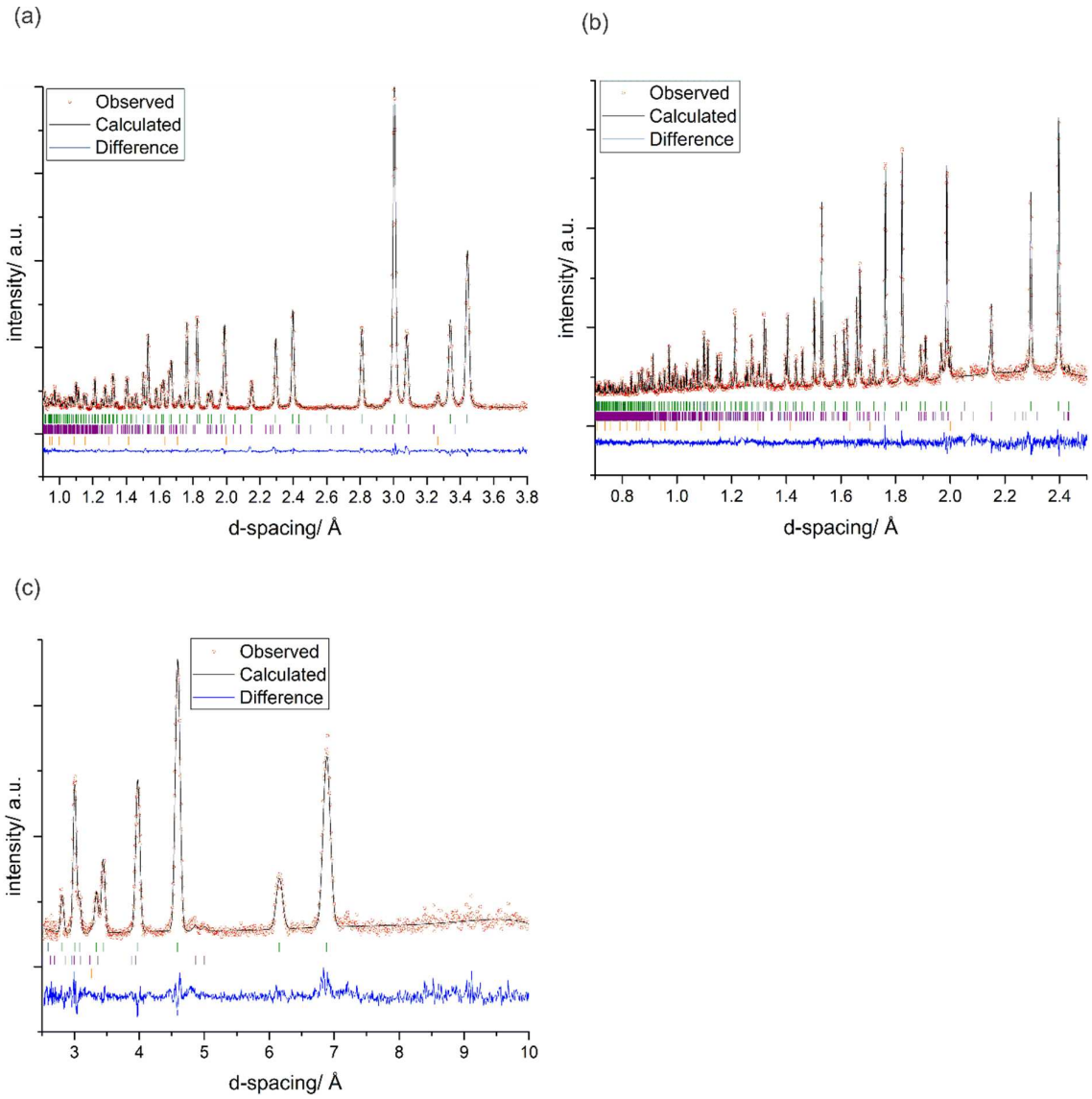

Figure S8: Ambient temperature Rietveld refinements of $^{7}Li_{4.4}Al_{0.4}Ge_{0.6}S_4$ (synthesised using purified reactants) against NPD data (ISIS neutron source, HRPD beam line), using the final NPD-derived model with three Li sites. The positons of calculated Bragg reflections are shown by tick marks (green: $^{7}Li_{4.4}Al_{0.4}Ge_{0.6}S_4$, purple: $LiAlS_2$, orange: Ge) (a) Bank 1, 2θ = 169°, (b) Bank2, 2θ = 90° (c) Bank 3, 2θ = 30°.

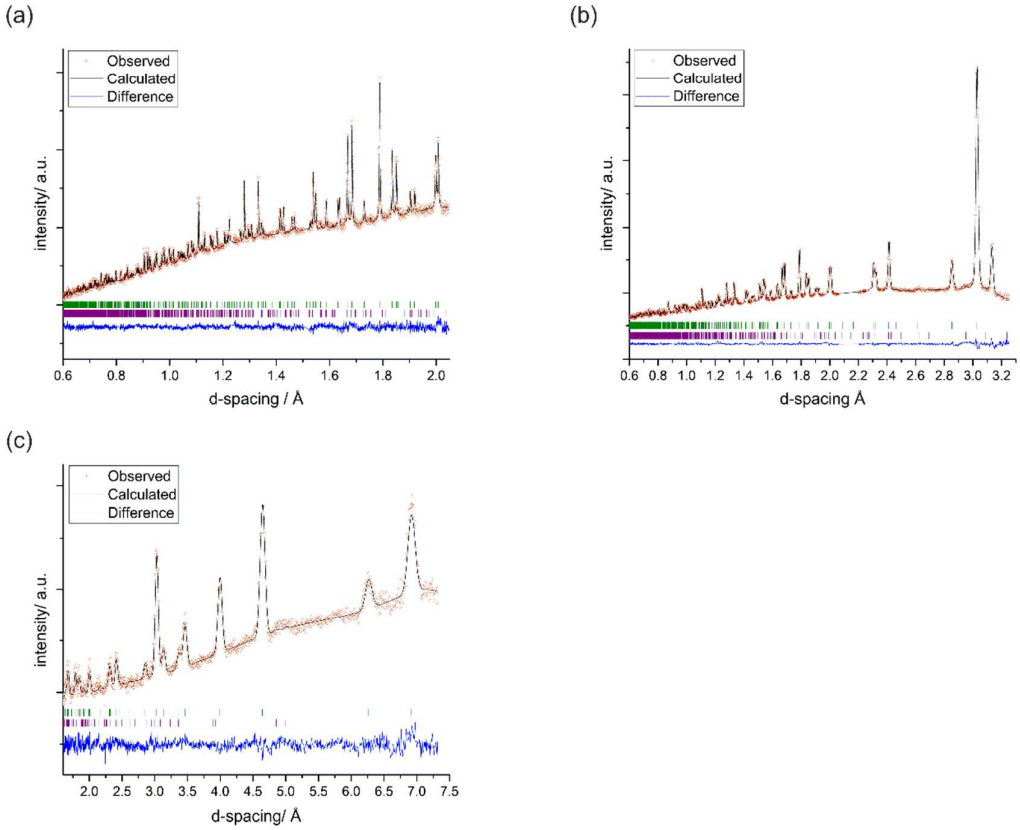

Figure S9: Low temperature Rietveld refinements of $^{7}Li_{4.4}Al_{0.4}Sn_{0.6}S_4$ (synthesised using purified reactants) against NPD data (ISIS neutron source, HRPD line, T= 10 K). The positions of calculated Bragg reflections are shown by tick marks (green: $^{7}Li_{4.4}Al_{0.4}Sn_{0.6}S_4$, purple: $LiAlS_2$). (a) Bank 1, 2θ = 169° (b) Bank 2, 2θ = 90° (c) Bank3, 2θ = 30°.

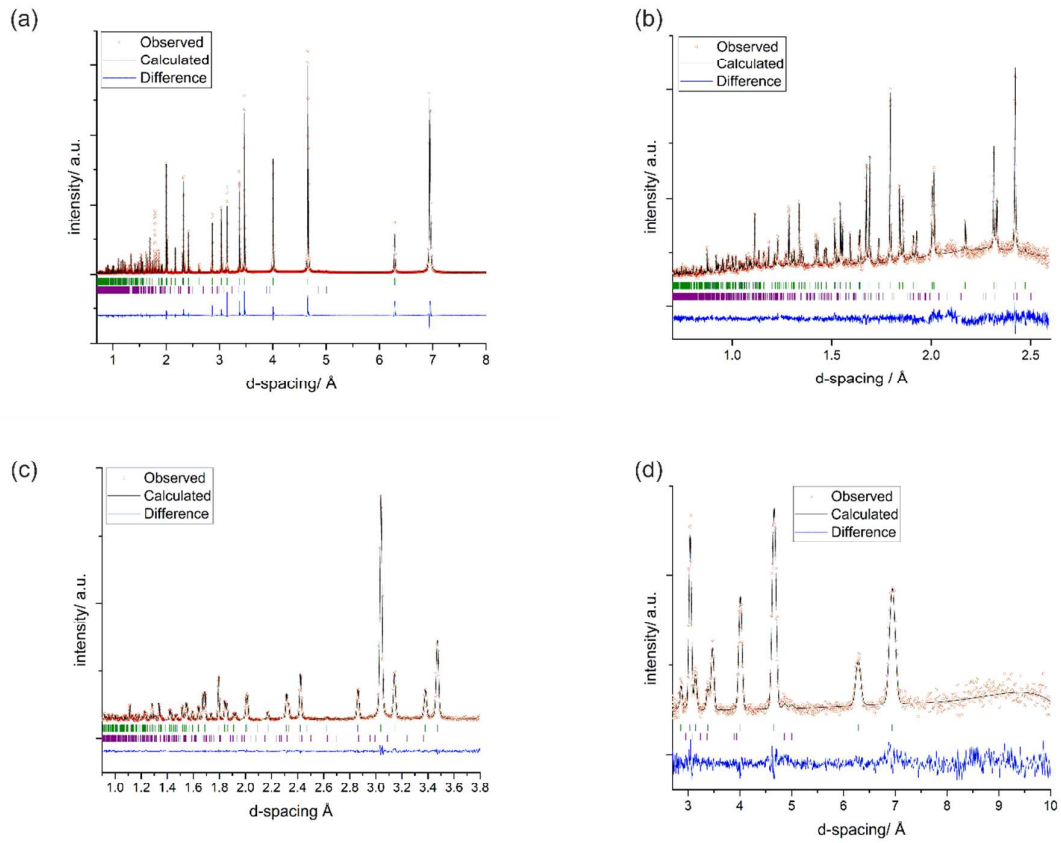

Figure S10: Ambient temperature Rietveld refinements of $^{7}Li_{4.4}Al_{0.4}Sn_{0.6}S_4$ (synthesised using purified reactants) against SXRD data (I11 beamline, MAC-detector, λ= 0.824878 Å) and NPD data (ISIS neutron source, HRPD beam line). The positons of calculated Bragg reflections are shown by tick marks (green = $^{7}Li_{4.4}Al_{0.4}Sn_{0.6}S_4$, purple = $LiAlS_2$). (a) SXRD pattern, (b) NPD pattern, Bank 1, 2θ = 169°, (c) NPD pattern, Bank2, 2θ = 90° (d) NPD pattern, Bank 3, 2θ = 30°.

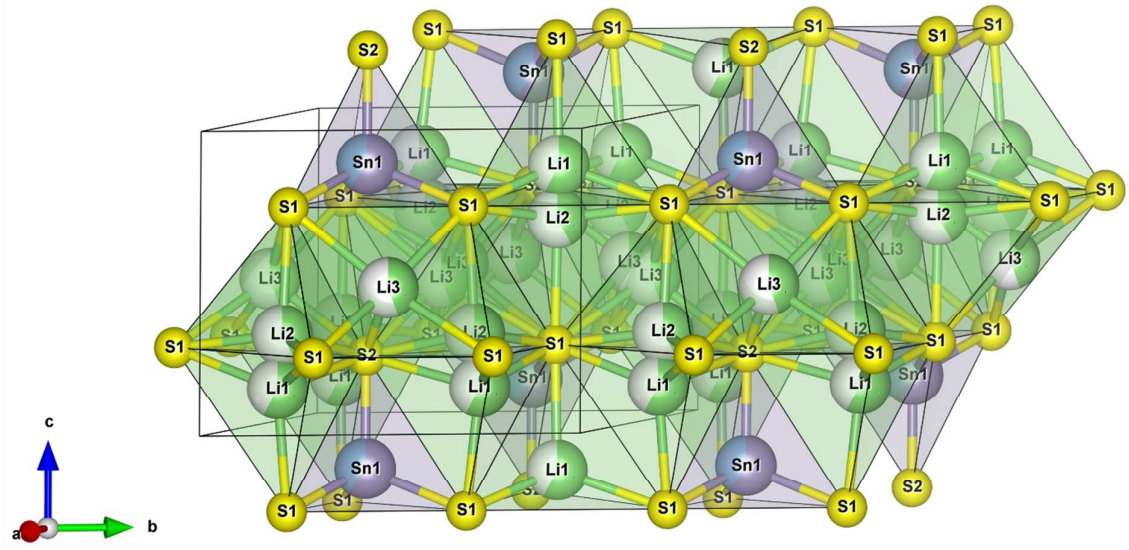

Figure S11: Crystal structure of $Li_{4.4}Al_{0.4}Sn_{0.6}S_4$ at 10 K. There are two sites in the tetrahedral layer, one occupied by Li1/vacancies and the other by Al/Sn. In the octahedral layer Li2 and Li3 can be found in tetrahedral and octahedral

interstices respectively. Atoms and polyhedra are coloured as follows: yellow: sulphur, green = lithium, blue = aluminium and purple = tin. Partially occupied atoms are coloured to represent fractional occupancies.

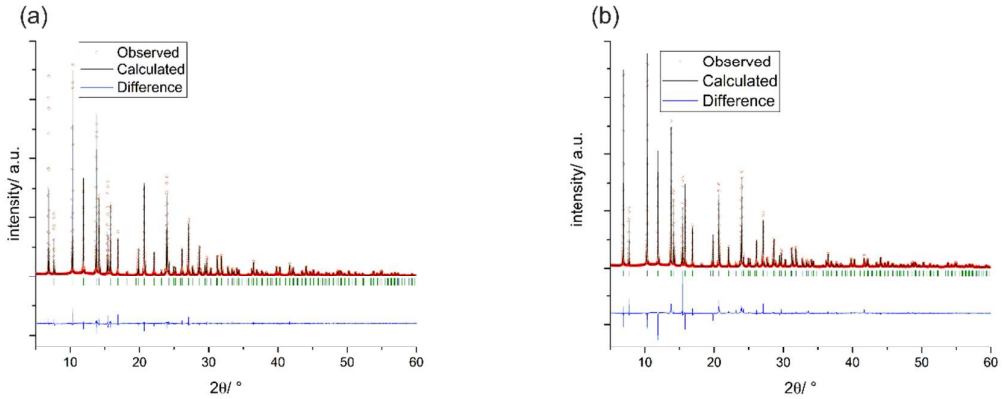

Figure S12: Refinement of $Li_{4.4}Ga_{0.4}Ge_{0.6}S_4$ (synthesised using purified reactants) against SXRD data (I11 beamline, MAC-detector, λ= 0.824868(1) Å, room temperature). The positons of calculated Bragg reflections are shown by green tick marks. (a) Pawley fit: R_{wp}=6.37, χ^2= 20.62. (b) Rietveld fit: R_{wp}= 9.62, χ^2= 45.75.

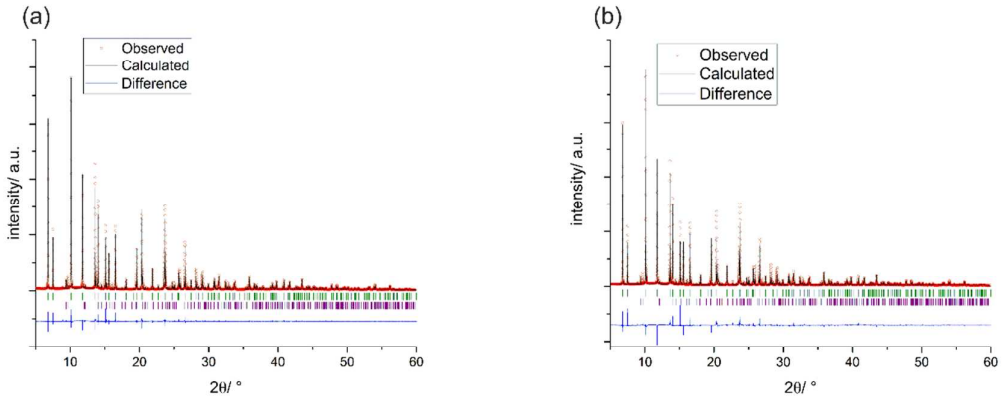

Figure S13: Refinement of $Li_{4.4}Ga_{0.4}Sn_{0.6}S_4$ (synthesised using purified reactants) against SXRD data (I11 beamline, MAC-detector, λ= 0.824868(1) Å, room temperature). The positons of calculated Bragg reflections are shown by tick marks (green: $Li_{4.4}Ga_{0.4}Sn_{0.6}S_4$, purple: $LiGaS_2$). (a) Pawley fit: R_{wp}: 6.29, χ^2= 16.56 (b): Rietveld fit: R_{wp}= 8.55, χ^2= 28.59

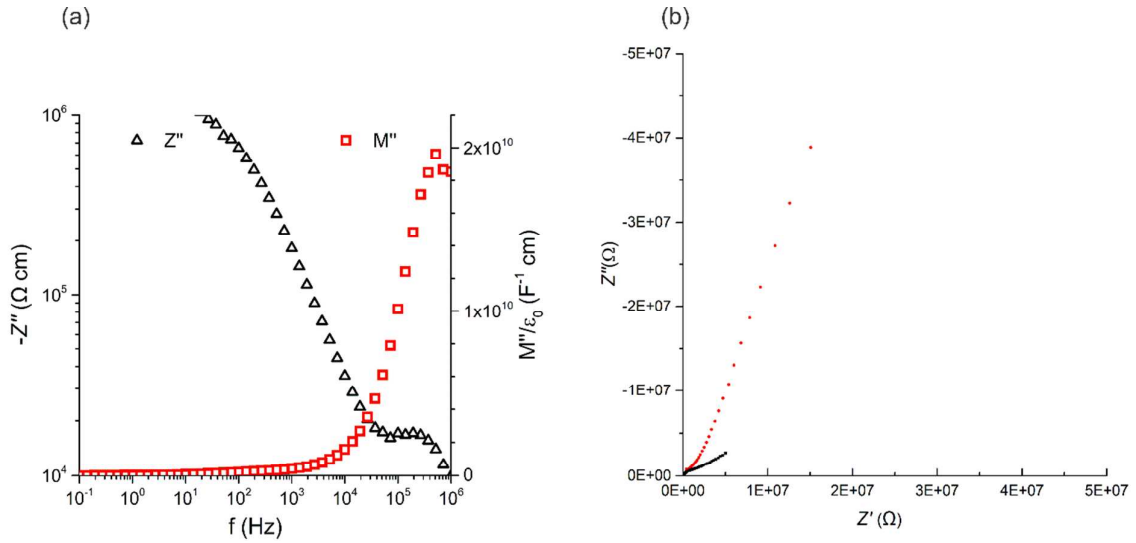

Figure S14: (a) Modulus plot of AC-impedance experiment on $Li_{4.4}Al_{0.4}Ge_{0.6}S_4$. (b) Full AC-impedance plot of $Li_{4.4}Al_{0.4}Ge_{0.6}S_4$ (black) and $Li_{4.4}Al_{0.4}Sn_{0.6}S_4$ (red) measured from 1MHz to 100 mHz at 303 K.

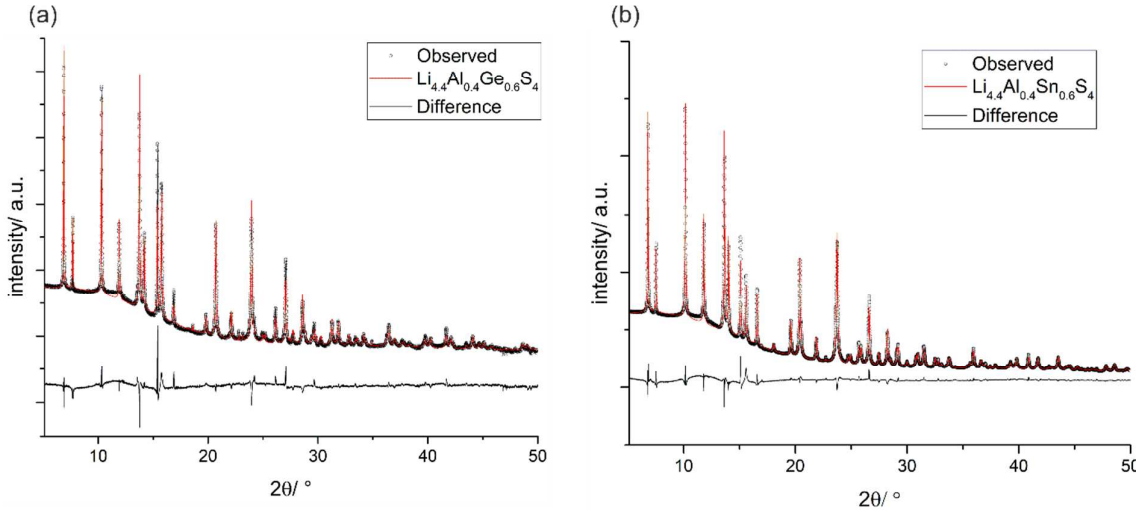

Figure S15: Rietveld refinements of solid electrolytes against SXRD data after cycling against lithium metal showing that the bulk structure of each compound has been retained after cycling. (a) $Li_{4.4}Al_{0.4}Ge_{0.6}S_4$ (b) $Li_{4.4}Al_{0.4}Sn_{0.6}S_4$. (I11 beamline, PSD-detector, λ= 0.825015 Å, room temperature).

$Li_{4.4}Al_{0.4}Ge_{0.6}S_4$

Figure S16: Cu-electrode of Li|SE|Cu cell after plating experiment, showing evidence for lithium metal plating.

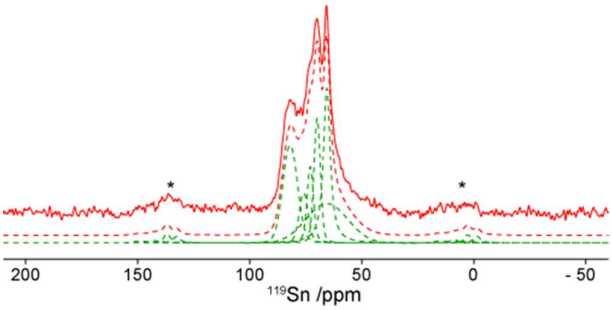

Figure S17: ^{119}Sn MAS NMR spectrum of $Li_{4.4}Al_{0.4}Sn_{0.6}S_4$ at MAS rate of 10 kHz. Red dotted line represents the sum of the simulated peaks (dotted green). Asterisks (*) denote spinning sidebands.

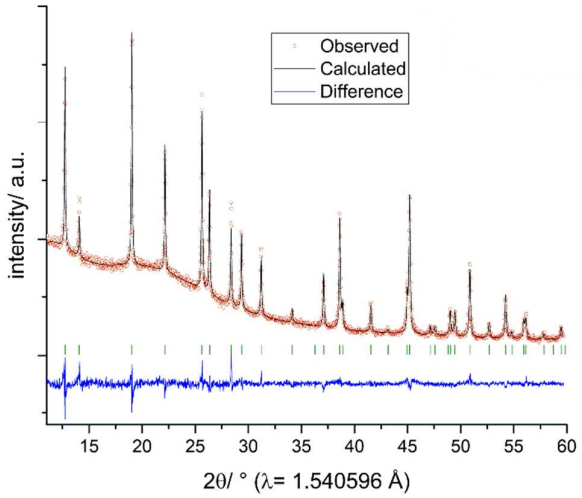

Figure S18: Rietveld refinement of $Li_{4.4}Al_{0.4}Sn_{0.6}S_4$ used for solid state NMR against lab PXRD data (λ = 1.540596 Å). The positions of calculated Bragg reflections are shown by green tick marks.

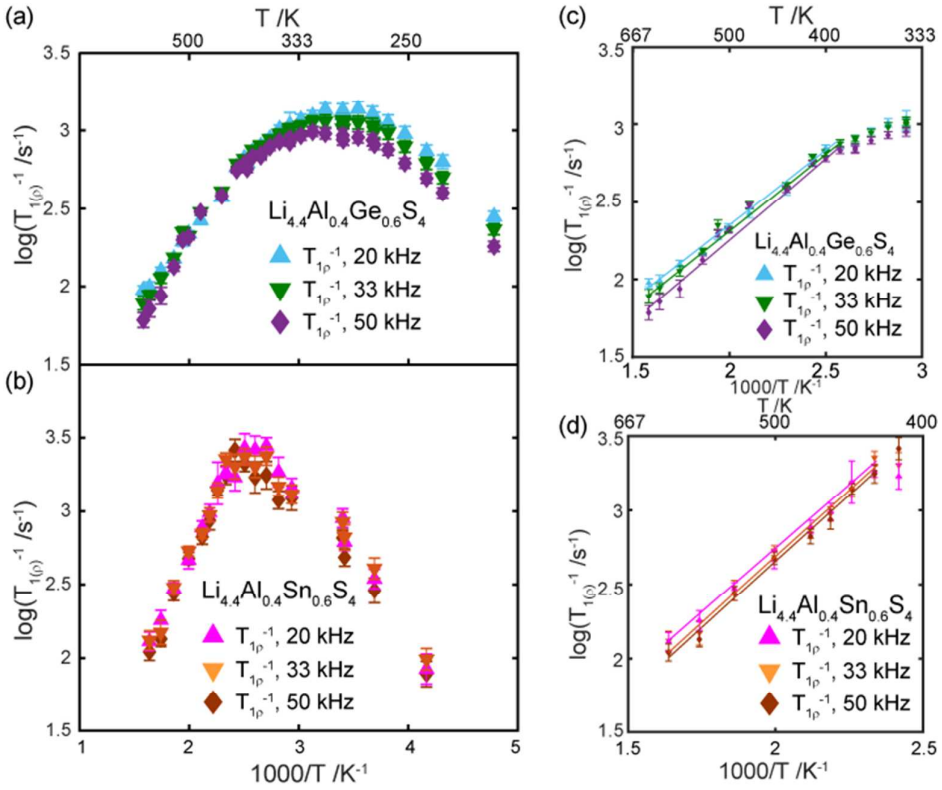

Figure S19: (a-b) Arrhenius plots of ^7Li $T_{1\rho}^{-1}$ spin-lattice relaxation rates (SLR) around the maxima values. (c-d) Zoomed view of the high temperature flank show the spin-lock frequency dependence of SLR rates. See Figure 12 (main text) for further details.

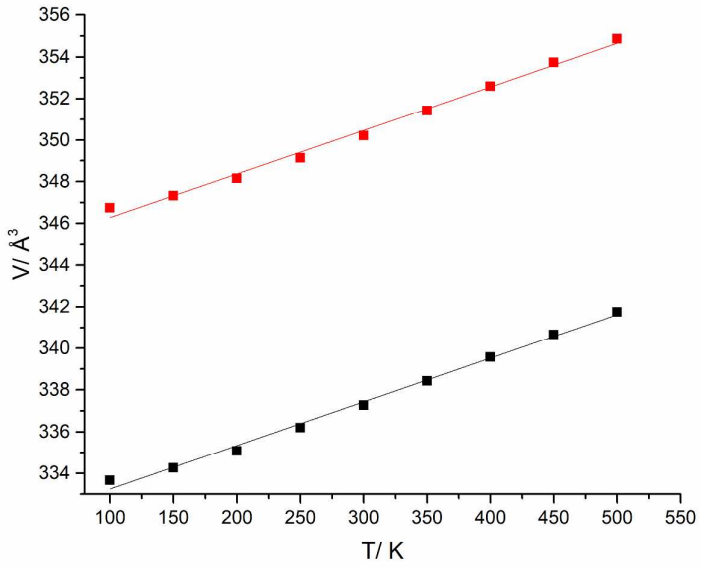

Figure S20. Temperature dependence of the unit cell volume of $Li_{4.4}Al_{0.4}Ge_{0.6}S_4$ (black) and $Li_{4.4}Al_{0.4}Sn_{0.6}S_4$ (red), determined by Pawley fitting to variable-temperature SXRD data (I11, position sensitive detector).

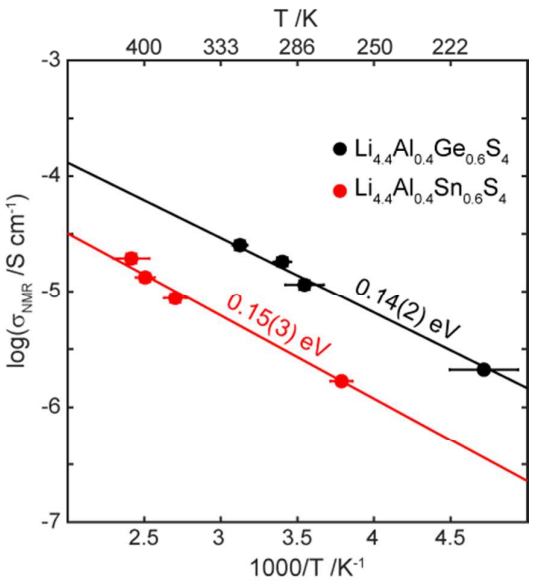

Figure S21: Arrhenius plot of NMR conductivity of $Li_{4.4}Al_{0.4}Ge_{0.6}S_4$ (black) and $Li_{4.4}Al_{0.4}Sn_{0.6}S_4$ (red). Horizontal error bars denote the sample temperature gradient in the NMR probe.

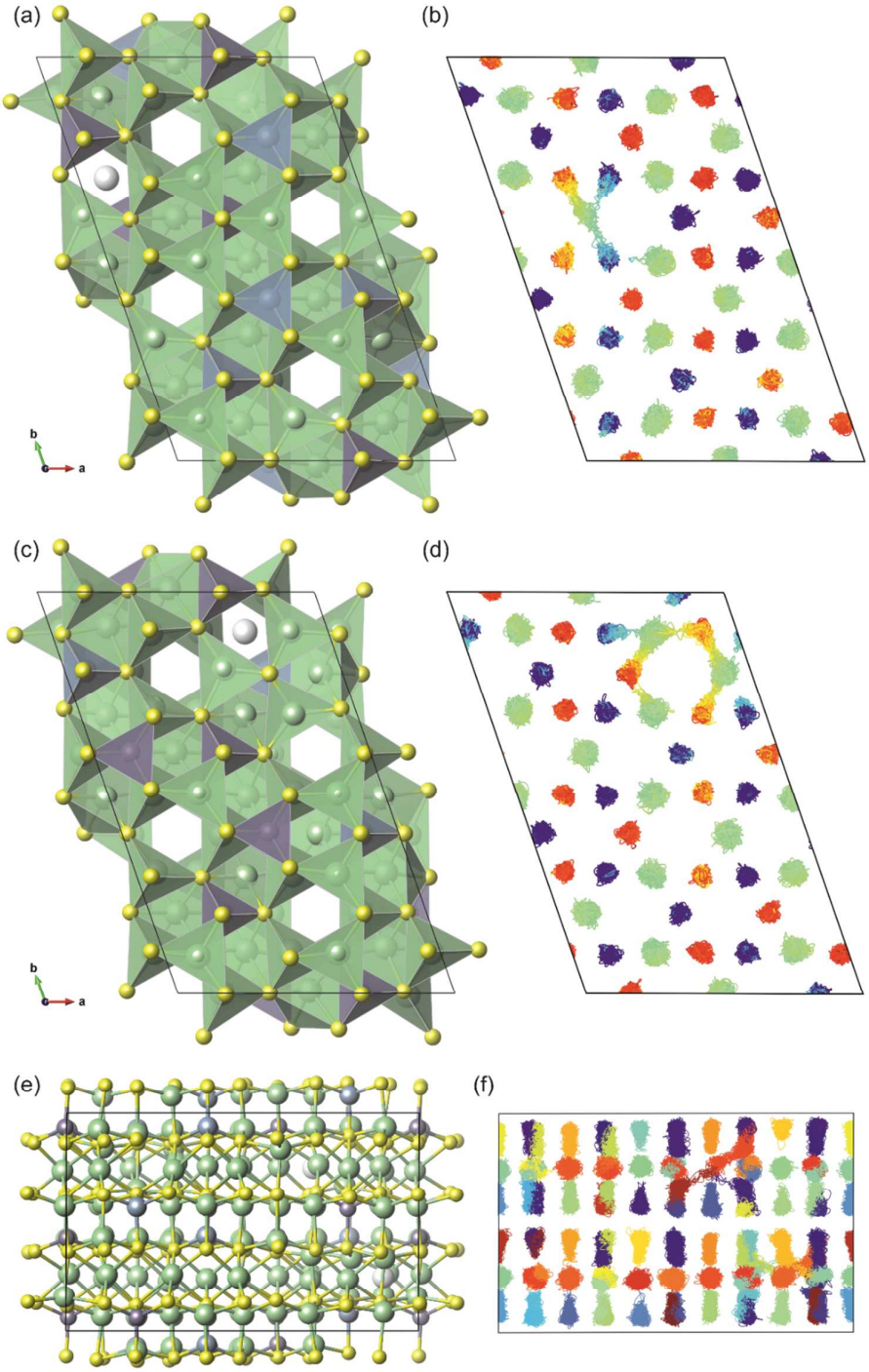

Figure S22: The AIMD trajectory of Li ions in supercell A. (a) shows the view down the c axis of top half of supercell A before the AIMD trajectory begins (yellow: sulphur, green: lithium, blue: aluminium and purple: germanium), with the initially vacant Li3 site shown as a gray sphere. (b) shows the Li ion positions in this top half of the cell throughout the 88 ps AIMD trajectory. Atoms are coloured according to position along c, with (pseudo)octahedral sites in green, and tetrahedral in blues and reds. (c) shows the view down the c axis of bottom half of supercell A before the AIMD trajectory begins (Li: green, Al: blue, Ge: purple, S: yellow), with the initially vacant Li3 site shown as a white sphere. (d) shows the Li ion positions in this bottom half of the cell throughout the 88 ps AIMD trajectory. Atoms are coloured according to position along c, with (pseudo)octahedral sites in green, and tetrahedral in blues and reds. (e) shows a view down the a axis of supercell A before the AIMD trajectory begins. (f) shows the Li ion positions viewed down the same axis throughout the 88 ps AIMD trajectory with each atom's positions shown in a different colour.

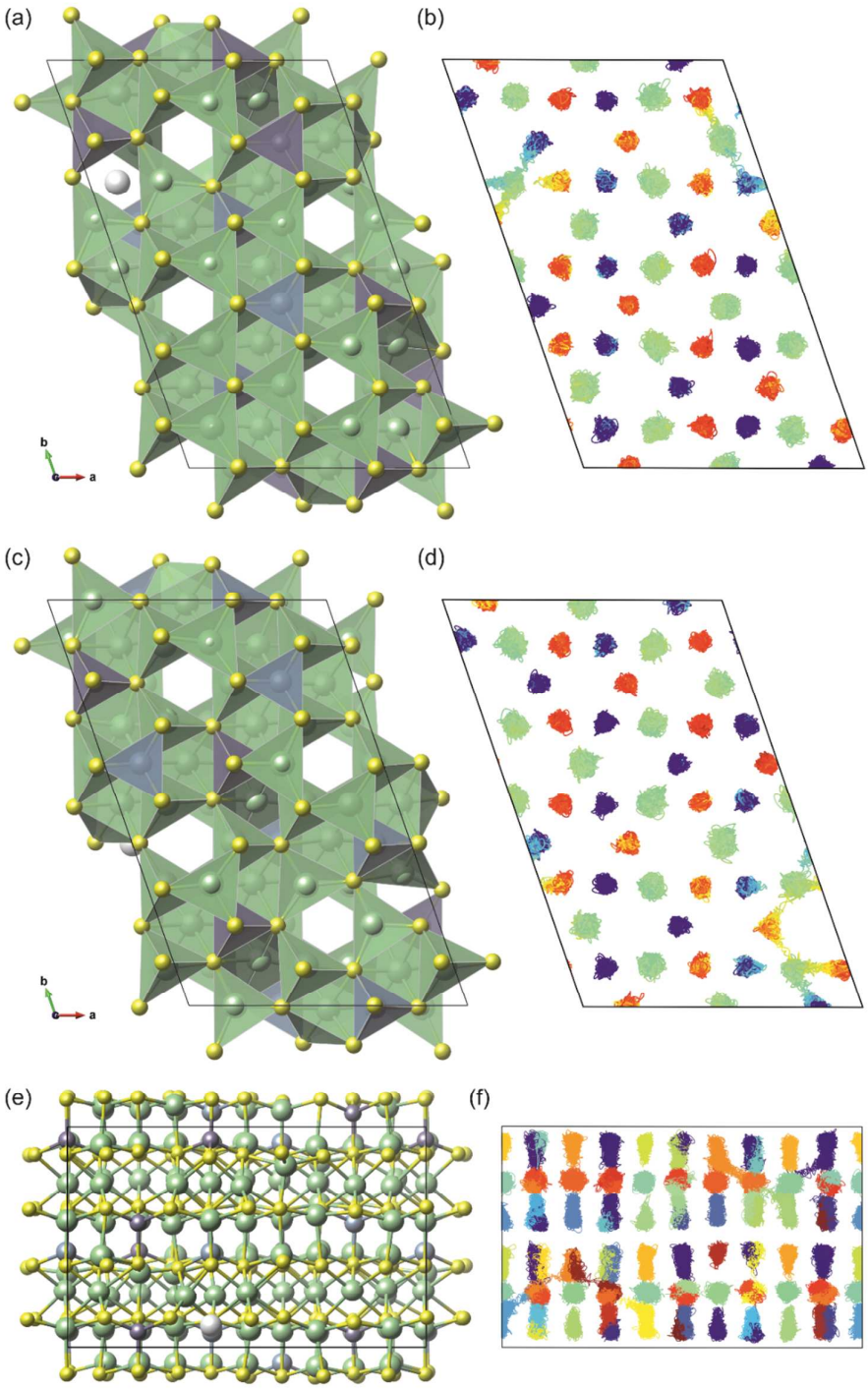

Figure S23: The AIMD trajectory of Li ions in supercell B. (a) shows the view down the c axis of top half of supercell B before the AIMD trajectory begins (yellow: sulphur, green: lithium, blue: aluminium and purple: germanium), with the initially vacant Li3 site shown as a white sphere. (b) shows the Li ion positions in this top half of the cell throughout the 120 ps AIMD trajectory. Atoms are coloured according to position along c, with (pseudo)octahedral sites in green, and tetrahedral in blues and reds. (c) shows the view down the c axis of bottom half of supercell B before the AIMD trajectory begins (Li: green, Al: blue, Ge:purple, S:yellow), with the initially vacant Li3 site shown as a white sphere. (d) shows the Li ion positions in this bottom half of the cell throughout the 120 ps AIMD trajectory. Atoms are coloured according to position along c, with (pseudo)octahedral sites in green, and tetrahedral in blues and reds. (e) shows a view down the a axis of supercell B before the AIMD trajectory begins. (f) shows the Li ion positions viewed down the same axis throughout the 120 ps AIMD trajectory with each atom's positions shown in a different colour.

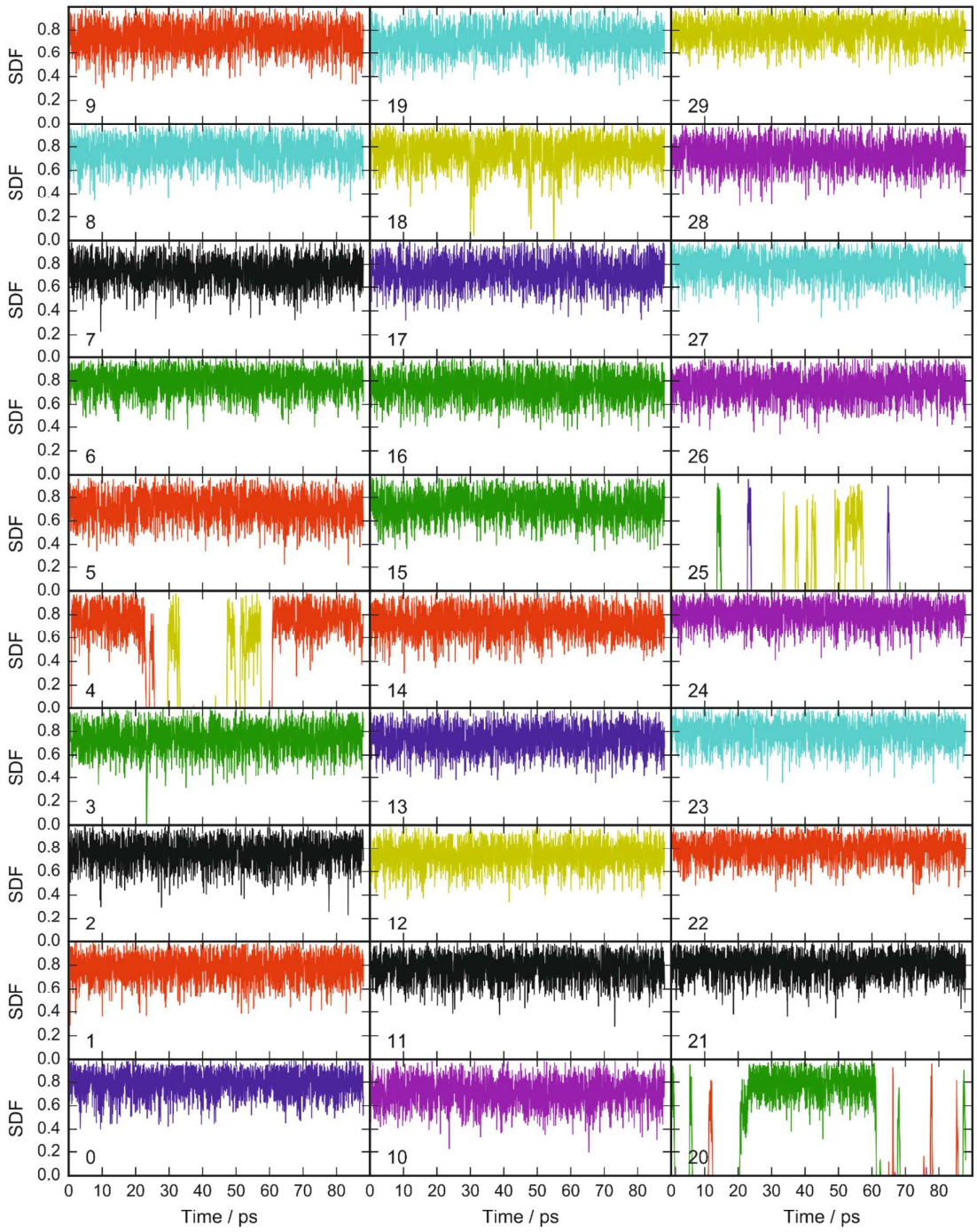

Figure S24: SDF plots of all thirty octahedral interstitial spaces in supercell A. A value of zero in the SDF means that the site is vacant, and a value of one that the Li atom is at the centre of the octahedral site. Different coloured lines represent different Li atoms in the AIMD calculation.

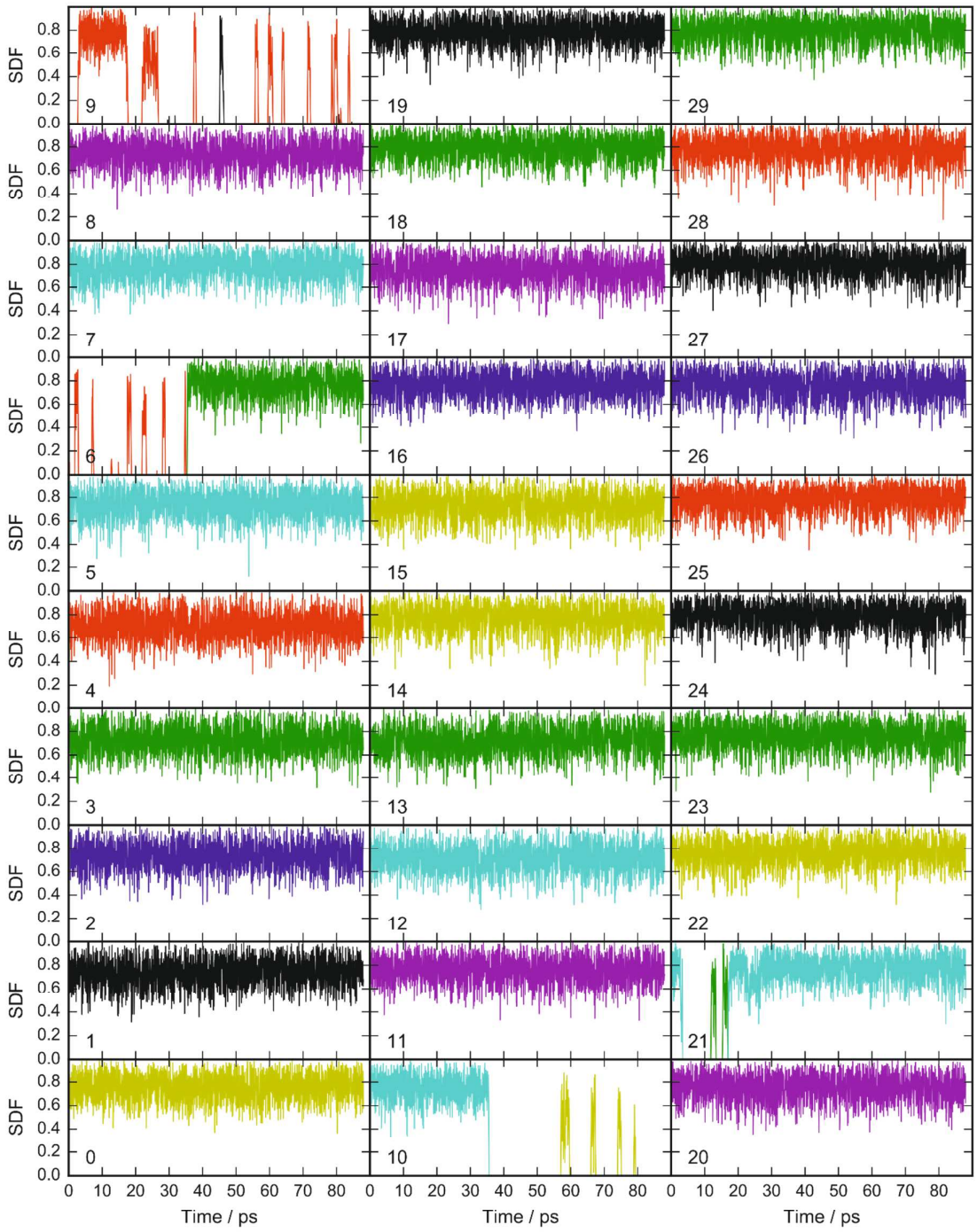

Figure S25: SDF plots of all thirty octahedral interstitial spaces in supercell B. A value of zero in the SDF means that the site is vacant, and a value of one that the Li atom is at the centre of the octahedral site. Different coloured lines represent different Li atoms in the AIMD calculation.

Table S1: The relative energies of the five lowest energy configurations of $Li_{88}Al_8Ge_{12}S_{80}$ supercells by "fast" DFT calculations, and their relative energies using the more accurate "slow" parameters. *Optimisation of supercell D with the "slow" parameters resulted in a new stable configuration with different occupation of Li sites. Recalculation of the energy of this new configuration with the "fast" settings results in an energy only 2 meV/cell above supercell A. Similarly recalculation of the energy of supercell E with "fast" settings, following optimisation with "slow" settings gives a relative energy of 132 meV above supercell A.

Supercell	$E-E_A$ (meV/cell) "Fast"	$E-E_A$ (meV/cell) "Slow"
A	0	0
B	65	53
C	122	124
D	160 (2*)	-6
E	188 (132*)	124

Table S2: Results of elemental analysis of $Li_{4.4}Al_{0.4}Ge_{0.6}S_4$ (synthesised using commercial Li_2S and Ge) – ICP-OES method.

Element	wt %	Normalised atomic ratios
Li	13.5	4.40(9)
Al	5.26	0.44(1)
Ge	20.6	0.64(1)
S	56.6	3.99(8)

Table S3: Results of elemental analysis of $Li_{4.4}Al_{0.4}Ge_{0.6}S_4$ (synthesised using commercial Li_2S and Ge) - combustion method. The presence of oxygen is consistent with the presence of Al_2O_3 in the PXRD pattern.

Element	Measured /wt %	Expected /wt%
C	< 0.1	0
H	< 0.1	0
O	1.97	0
S	58.7	59.9

Table S4: Structural parameters of $Li_{4.4}Al_{0.4}Ge_{0.6}S_4$ from a Rietveld refinement at 10 K using NPD data.

Atom	Wyckoff site	x	y	z	occupancy	$U_{iso}/Å^2$
S1	6i	0.18174(7)	0.36347(13)	0.26092(30)	1	0.00791(25)
S2	2d	1/3	2/3	-0.22674(30)	1	0.0034(4)
Ge1	2d	1/3	2/3	0.13408(18)	0.6	0.00532(18)
Al1	2d	1/3	2/3	0.13408(18)	0.4	0.00532(18)
Li1	6i	0.31591(35)	0.15794(18)	0.1557(5)	0.738(5)	0.0156(6)
Li3	6i	0.4871(4)	0.5129(4)	0.5159(13)	0.441(7)	0.0256(16)
Li2	6i	0.3394(10)	0.16973175(11)	0.254(4)	Uiso	0.0156(6)

a= 7.91914(6), *b*= 6.13319(7), Space group= $P\bar{3}m1$, R_{wp}= 0.0122, χ^2= 1.687, impurity phases: $LiAlS_2$ (2.0 wt%), Ge (0.4 wt%).

Table S5: Structural parameters of $Li_{4.4}Al_{0.4}Ge_{0.6}S_4$ from a Rietveld refinement at ambient temperature using NPD data.

Atom	Wyckoff site	x	y	z	occupancy	U_{iso}/Å^2
S1	6i	0.18173(7)	0.36346(13)	0.26202(27)	1	0.01863(35)
S2	2d	1/3	2/3	-0.22694(29)	1	0.0135(5)
Ge1	2d	1/3	2/3	0.13364(17)	0.595(4)	0.01443(25)
Al1	2d	1/3	2/3	0.13364(17)	0.405(4)	0.01443(25)
Li1	6i	0.3191(4)	0.15954(20)	0.1611(7)	0.767(6)	0.0330(7)
Li3	6i	0.48487(35)	0.51513(35)	0.5185(14)	0.461(5)	0.0420(15)
Li2	6i	0.3344(12)	0.1671(6)	0.3156(18)	0.221(5)	0.0330(7)

a= 7.94785(5), *b*= 6.15520(7), Space group= $P\bar{3}m1$, R_{wp}= 0.0275, χ^2= 2.044, impurity phases: $LiAlS_2$ (2.0 wt%), Ge (0.4 wt%).

Table S6: Results of elemental analysis of $Li_{4.4}Al_{0.4}Sn_{0.6}S_4$ (synthesised using in-house prepared phase-pure Li_2S) by ICP-OES.

Element	Measured concentration/ mg/L	Molar concentration mmol/L	Normalised atomic ratio
Li	12.8(1)	1.86(2)	4.40(4)
Al	4.87(7)	0.180(3)	0.43(1)
Sn	29.9(1)	0.252(1)	0.60(2)
S	x	x	x

Table S7: Structural parameters of $Li_{4.4}Al_{0.4}Sn_{0.6}S_4$ from a Rietveld refinement at 10 K using NPD data.

Atom	Wyckoff site	x	y	z	occupancy	U_{iso}/Å^2
S1	6i	0.17617(9)	0.35233(17)	0.26535(30)	1	0.01007(31)
S2	2d	1/3	2/3	-0.23562(33)	1	0.0102(4)
Sn1	2d	1/3	2/3	0.13475(24)	0.6	0.00687(24)
Al1	2d	1/3	2/3	0.13475(24)	0.4	0.00687(24)
Li1	6i	0.3118(4)	0.15589(22)	0.1431(6)	0.575(4)	0.0149(6)
Li3	6i	0.4835(4)	0.5165(4)	0.5202(13)	0.435(7)	0.0331(19)
Li2	6i	0.3302(6)	0.16504(32)	0.3189(6)	0.422(4)	0.0149(6)

a= 7.98832(6) Å, *b*= 6.2646(7) Å, Space group= $P\bar{3}m1$, R_{wp}= 0.0114, χ^2= 1.56, impurity phase: $LiAlS_2$ (1.5 wt%).

Table S8: Structural parameters of $Li_{4.4}Al_{0.4}Sn_{0.6}S_4$ from a Rietveld refinement at ambient temperature using NPD data.

Atom	Wyckoff site	x	y	z	occupancy	$U_{iso}/Å^2$
S1	6i	0.17658(8)	0.35315(16)	0.26304(27)	1	0.02224(35)
S2	2d	1/3	2/3	-0.23539(29)	1	0.0177(4)
Sn1	2d	1/3	2/3	0.13622(21)	0.6	0.01733(27)
Al1	2d	1/3	2/3	0.13622(21)	0.4	0.01733(27)
Li1	6i	0.3130(5)	0.15649(23)	0.1428(6)	0.584(4)	0.0293(6)
Li3	6i	0.4820(4)	0.5181(4)	0.5249(12)	0.460(5)	0.0573(18)
Li2	6i	0.3288(6)	0.16434(30)	0.3092(6)	0.4271(31)	0.0293(6)

a= 8.01711(6) Å, *b*= 6.26461(8) Å, Space group= $P\bar{3}m1$, R_{wp}= 0.0245, χ^2= 1.39, impurity phase: $LiAlS_2$ (1.5 wt%).

Table S9: Bond distances and distortion indices of MS_4 tetrahedra and octahedra in $Li_{4.4}Al_{0.4}Ge_{0.6}S_4$ at 10 K. Atoms marked with primes (') relate to Figure 5.

$Li_{4.4}Al_{0.4}Ge_{0.6}S_4$	Bond length/ Å			
	Al/Ge	Li1	Li2	Li3
S1	2.2201(9)	2.4338(17)	2.439(5)	2.614(6)
S1'	x	2.576(4)	2.591(7)	2.673(5)
S2	2.213(3)	2.4447(18)	2.312(6)	2.634(6)
S2'	x	x	x	3.035(6)
Coordination polyhedron	Tetrahedral	Tetrahedral	Tetrahedral	Octahedral
Distortion index/ dimensionless	0.00121	0.02101	0.02974	0.04039

Table S10: Bond distances and distortion indices of MS_4 tetrahedra and MS_6 octahedra in Li_5AlS_4 at ambient temperature.[1] Atoms marked with primes (') relate to Figure 5.

Li_5AlS_4	Bond length/ Å				
	Al	Li1	Li2	Li3	Li4
S1	2.2425(10)	2.3944(9)	2.638(13)	3.1389(12)	2.6562(5)
S2	2.2786(8)	2.4385(8)	2.382(14)	2.5934(11)	2.8508(5)
S3	2.2901(6)	2.3465(10)	2.433(7)	2.5541(7)	2.7284(6)
S3'	x	2.5657(11)	x	2.9100(8)	x
Coordination polyhedron	Tetrahedral	Tetrahedral	Tetrahedral	Octahedral	Octahedral
Distortion index/ dimensionless	0.00722	0.02702	0.03370	0.06085	0.02567

Table S11: Bond distances and distortion indices of MS_4 tetrahedra and MS_6 octahedra in Li_4GeS_4 at ambient temperature.[2] Atoms marked with primes (') relate to Figure 5.

Li_4GeS_4	Bond length/ Å			
	Ge	Li1	Li2	Li3
S1	2.2168(12)	2.9094(9)	2.493(4)	2.406(3)
S2	2.2096(12)	2.5894(14)	2.4503(19)	2.383(4)
S2'	x	x	x	2.576(3)
S3	2.228(4)	2.5572(11)	2.498(4)	2.550(4)
Coordination polyhedron	Tetrahedral	Octahedral	Tetrahedral	Tetrahedral
Distortion index/ dimensionless	0.00289	0.05563	0.00914	0.03398

Table S12: Bond distances and distortion indices of MS_4 tetrahedra and MS_6 octahedra in $Li_{4.4}Al_{0.4}Sn_{0.6}S_4$ at 10 K.

$Li_{4.4}Al_{0.4}Sn_{0.6}S_4$	Bond length/ Å			
	Al/Sn	Li1	Li2	Li3
S1	2.3251(11)	2.435(4)	2.386(4)	2.662(6)
S1	x	2.572(5)	2.613(5)	2.730(6)
S2	2.321(4)	2.519(3)	2.386(4)	2.673(6)
S2	x	x	x	3.105(6)
Coordination polyhedron	Tetrahedral	Tetrahedral	Octahedral	Octahedral
Distortion index/ dimensionless	0.00072	0.02225	0.03475	0.04393

Table S13: Structural parameters of $Li_{4.4}Ga_{0.4}Ge_{0.6}S_4$ from a Rietveld refinement against room temperature SXRD data only, modelled without any lithium sites (I11 beamline, MAC-detector, λ= 0.824868(1) Å). Only the lattice parameters of the unit cell, the positions of the heavy atoms and thermal parameters were refined. The occupancy of sulfur and the combined Ga/Ge site were fixed to one respectively.

Atom	Wyckoff site	x	y	z	Occupancy	U_{iso}/Å^2
S1	6i	0.17907(8)	0.3581(2)	0.2629(2)	1	0.0138(5)
S2	2d	1/3	2/3	0.7638(3)	1	0.0105(6)
Ga	2d	1/3	2/3	0.1317(2)	0.4	0.0102(4)
Ge	2d	1/3	2/3	0.1317(2)	0.6	0.0102(4)

a= 7.94866(6) Å, *c*= 6.1521(2) Å, Space group= $P\bar{3}m1$, R_{wp}= 9.62, χ^2= 45.75.

Table S14: Structural parameters of $Li_{4.4}Ga_{0.4}Sn_{0.6}S_4$ from a Rietveld refinement against room temperature SXRD data only, modelled without any lithium sites (I11 beamline, MAC-detector, λ= 0.824868(1) Å). Only the lattice parameters of the unit cell, the positions of the heavy atoms and thermal parameters were refined. The occupancy of sulphur and the combined Ga/Sn site were fixed to one respectively.

Atom	Wyckoff site	x	y	z	Occupancy	U_{iso}/Å^2
S1	6i	0.17499(8)	0.3499(2)	0.2665(2)	1	0.0163(4)
S2	2d	1/3	2/3	0.7564(3)	1	0.0129(5)
Ga	2d	1/3	2/3	0.1319(1)	0.4	0.0159(4)
Sn	2d	1/3	2/3	0.1319(1)	0.6	0.0159(4)

a= 8.0296(8) Å, *c*= 6.2851(7) Å, Space group= $P\bar{3}m1$, R_{wp}= 8.55, χ^2= 28.59, impurity phase: $LiGaS_2$ (3.5 wt%).

Table S15: Conductivities, capacitances and relative permittivities of $Li_{4.4}M_{0.4}M'_{0.6}S_4$ (*M*= Al, Ga and *M'*= Ge, Sn) calculated from AC-impedance spectroscopy data.

Material	Conductivity/ S cm^{-1}	Capacitance/ F cm^{-1}	Relative permittivity ε_R
$Li_{4.4}Al_{0.4}Ge_{0.6}S_4$	4.3(3) x 10^{-5}	8.68 x 10^{-10}	9803
$Li_{4.4}Al_{0.4}Sn_{0.6}S_4$	4.3(9) x 10^{-6}	5.96 x 10^{-11}	673
$Li_{4.4}Ga_{0.4}Ge_{0.6}S_4$	1.6(3) x 10^{-5}	1.8 x 10^{-10}	2033
$Li_{4.4}Ga_{0.4}Sn_{0.6}S_4$	3(2)x10^{-6}	2.99 x 10^{-11}	338

References

1. Lim, H.; Kim, S. C.; Kim, J.; Kim, Y. I.; Kim, S. J., Structure of Li_5AlS_4 and comparison with other lithium-containing metal sulfides. *J. Solid State Chem.* **2018,** *257*, 19-25.
2. MacNeil, J. H.; Massi, D. M.; Zhang, J. H.; Rosmus, K. A.; Brunetta, C. D.; Gentile, T. A.; Aitken, J. A., Synthesis, structure, physicochemical characterization and electronic structure of thio-lithium super ionic conductors, Li_4GeS_4 and Li_4SnS_4. *J. Alloys Compd.* **2014,** *586*, 736-744.